ACS Chemical Neuroscience

pubs.acs.org/chemneuro Research Article

Pore Formation by Amyloid-like Peptides: Effects of the Nonpolar−Polar Sequence Pattern

Warin Rangubpit, Siwaporn Sungted, Jirasak Wong-Ekkabut, Hannah E. Distaffen, Bradley L. Nilsson, and Cristiano L. Dias*

Cite This: ACS Chem. Neurosci. 2024, 15, 3354−3362 Read Online

ACCESS | Metrics & More | Article Recommendations | Supporting Information

ABSTRACT: One of the mechanisms accounting for the toxicity of amyloid peptides in diseases like Alzheimer's and Parkinson's is the formation of pores on the plasma membrane of neurons. Here, we perform unbiased all-atom simulations of the full membrane damaging pathway, which includes adsorption, aggregation, and perforation of the lipid bilayer accounting for pore-like structures. Simulations are performed using four peptides made with the same amino acids. Differences in the nonpolar−polar sequence pattern of these peptides prompt them to adsorb into the membrane with the extended conformations oriented either parallel [peptide labeled F1, Ac-$(FKFE)_2$-NH_2], perpendicular (F4, Ac-FFFFKKEE-NH_2), or with an intermediate orientation (F2, Ac-FFKKFFEE-NH_2, and F3, Ac-FFFKFEKE-NH_2) in regard to the membrane surface. At the water−lipid interface, only F1 fully self-assembles into β-sheets, and F2 peptides partially fold into an α-helical structure. The β-sheets of F1 emerge as electrostatic interactions attract neighboring peptides to intermediate distances where nonpolar side chains can interact within the dry core of the bilayer. This complex interplay between electrostatic and nonpolar interactions is not observed for the other peptides. Although β-sheets of F1 peptides are mostly parallel to the membrane, some of their edges penetrate deep inside the bilayer, dragging water molecules with them. This precedes pore formation, which starts with the flow of two water layers through the membrane that expand into a stable cylindrical pore delimited by polar faces of β-sheets spanning both leaflets of the bilayer.

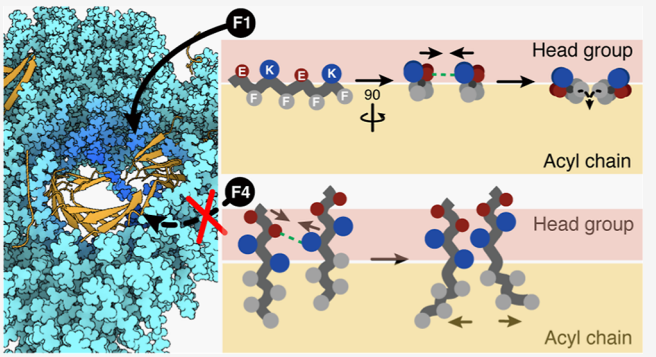

KEYWORDS: *amyloid, lipid membrane, membrane damage, pore formation, sequence pattern, permeation*

INTRODUCTION

One of the hallmarks of amyloid diseases is the aggregation of peptides into fibril-like structures in the intracellular or extracellular space of different tissues and organs.[1−3] This process disrupts the integrity of the plasma membrane, accounting for ion permeation that contributes to cellular dysfunction.[4,5] In the same vein, amyloid peptides can function as natural antibiotics by destroying the cell wall of invasive bacteria, suggesting that they play a role in our immune system.[6−10] Thus, understanding the molecular mechanisms of membrane damage by amyloids will not only enable our ability to design compounds that can inhibit the formation of toxic structures but also allow us to engineer better antimicrobial peptides. Despite extensive studies, these mechanisms remain mostly unknown. In silico studies have the potential to fill this knowledge gap.

General insights into the kinetics and thermodynamics of amyloid aggregation in solution and on the surface of lipid membranes have been obtained using coarse-grained models.[11−19] Some of these insights are supported by experiments including the role played by hydrophobic interactions in the nucleation process.[14,20] However, an atomistic understanding of amyloid-induced membrane damage is required to develop new strategies to interfere with the damaging process. Recent all-atom simulations have successfully described the formation of transient pores by α-helical antimicrobial peptides.[21−24] The structure of these α-helices is preserved throughout the poration process, which makes them easier to simulate than amyloids.[25] The latter undergo conformational changes in which bonds are formed and broken to account for β-sheets with the correct interhydrogen bond registry. Accordingly, most all-atom simulations in explicit solvent are performed starting with a preformed amyloid pore on the membrane surface.[26] By comparing different pore structures modeled as

Received: May 31, 2024
Revised: August 6, 2024
Accepted: August 9, 2024
Published: August 22, 2024

β-barrels, these studies provide insights into the most stable hydrogen bond registry.[27−30]

All-atom simulations also show that the competition between peptide−peptide and peptide−lipid interactions is critical to account for amyloid aggregation on the surface of lipid membranes.[31−34] Although this is consistent with experimental studies reporting a strong dependence of amyloid aggregation rates on lipid composition and membrane phase (gel versus fluid),[35−39] the interplay between different intermolecular interactions remains poorly understood. Unbiased all-atom simulations could shed light into this interplay and provide insights into pathways leading to pore formation.[40] This type of simulation has been achieved recently for short amphipathic peptides with the sequence Ac-$(FKFE)_2$-NH_2, in which nonpolar (phenylalanine, F) and polar (positive lysine, K, and negative glutamate, E) amino acids alternate along the sequence.[31]

In solution, the Ac-$(FKFE)_2$-NH_2 peptide, named F1 in this study, self-assembles into the characteristic cross-β signature of amyloid fibrils.[41,42] Cryogenic electron microscopy experiments have shown that this one-dimensional structure emerges from the concentric distribution of 4−5 twisted fibrils around a main axis, forming nanotubes.[43] Surprisingly, one of the β-sheets accounting for the cross-β pattern is antiparallel, while the other is parallel. All-atom simulations have been used to study the formation of cross-β fibrils by F1 peptides[40,44−46] and how they interact with lipid membranes.[31,47,48] Electrostatic interactions account for the attraction of F1 peptides to the vicinity of lipid membranes, whereas adsorption emerged from the burial of nonpolar phenylalanine into the dry core of the bilayer.[47,48] Accordingly, the attraction of F1 peptides to lipid membranes is significantly reduced by the presence of divalent ions,[48,49] which are promptly adsorbed onto phospholipid membranes.[50] This increases their concentration in solution, which could explain why calcium increases amyloid aggregation in the presence of lipid vesicles.[51,52] In all-atom simulations, adsorbed F1 peptides were shown to interact with each other, forming β-sheets on the membrane surface.[31] Moreover, β-sheets (either on the same or on opposite leaflets of the bilayer) were shown to interact with each other, leading to their penetration onto the membrane, accounting for stable pores.

Here, we provide insights into how the nonpolar−polar sequence pattern affects the pathways and interactions accounting for pore formation by studying four peptides made with the same amino acids distributed at different positions along the chain. Sequences of three of these peptides were constructed to allow the segregation of nonpolar and polar residues across the membrane−water interface when the peptide adopts an extended conformation oriented parallel (F1 peptide), perpendicular (Ac-FFFFKKEE-NH_2, F4), or with an intermediate orientation (Ac-FFFKFEKE-NH_2, F3) in regard to the membrane surface. The sequence of the fourth peptide is constructed in order to allow nonpolar and polar residues to segregate to opposite faces of a helical wheel (Ac-FFKKFFEE-NH_2, F2). Figure 1 illustrates these different segregation patterns. Our unbiased simulations show that, except for F1, all other peptides remain dispersed on the membrane interface after very long (>5 μs) simulations. Only F1 peptides that are oriented parallel to the membrane surface aggregate into β-sheets, which in turn self-assemble, forming pore-like structures on the lipid bilayer. Insights into the mechanisms of pore formation are provided by analyzing these simulations.

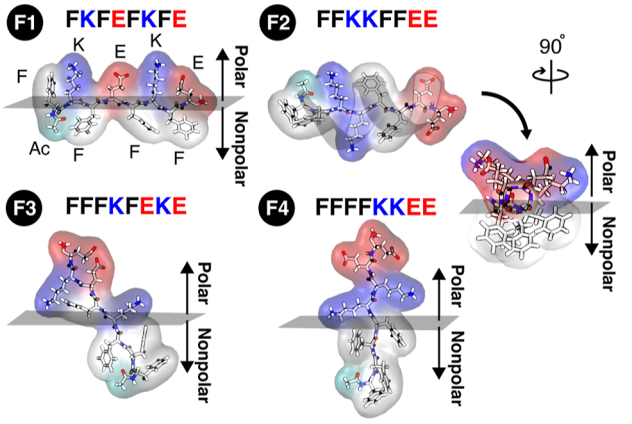

Figure 1. Atomic representation of the nonpolar−polar sequence patterns of peptides F1, F2, F3, and F4. In an extended conformation, peptides F1 and F4 segregate phenylalanine (F, white) from lysine (K, blue) and glutamic acid (E, red) at the water−lipid interface with their backbone oriented parallel and perpendicular to the membrane surface, respectively. Segregation takes place when the F3 peptide adopts an intermediate orientation with respect to the membrane and the F2 peptide folds into an α-helix.

In particular, a complex interplay between nonpolar and polar interactions is found to be critical in driving the formation of β-sheets. Moreover, the natural twist of the latter structures enables water molecules to penetrate deep inside the bilayer, driving the formation of a pore.

RESULTS AND DISCUSSION

Membrane damage requires peptides to adsorb and aggregate on the membrane surface. These aggregates can form structures that either extract lipids from the bilayer in a detergent-like manner or allow ions to permeate the membrane via the formation of pore-like structures on its surface.[4,5,9,52−57] These mechanisms of membrane damage are affected by the initial peptide concentration, which determines the size and structure of the aggregates that interact with the lipid membrane. For example, at high concentrations, F1 promptly forms fibrils in solution,[44] which were shown not to significantly affect the integrity of lipid bilayers.[31] Conversely, it was hypothesized that, at low concentrations, F1 forms only small nonfibrillar aggregates before interacting with lipid membranes. In computer simulations, the latter were shown to interfere promptly with the integrity of lipid membranes, creating pores on their surface.[31] This is consistent with the putative mechanism of membrane damage by amyloid peptides, wherein mostly oligomers are toxic as opposed to fibrils or monomers. Notice that amyloid peptides may not require the presence of a lipid membrane to form aggregates with pore-like structures as this type of conformation has been reported in all-atom simulations for the Aβ peptide in solution.[58]

Simulating the assembly of amyloid-like peptides into pore-like structures on the membrane surface requires using large boxes containing peptides at a concentration of the order of a few micromolars, which is the typical concentration used experimentally. Since 40 peptides are typically needed to damage membranes made with 200 lipids (i.e., 1:5 peptide/lipid ratio) in the time scale of a few microseconds,[31] this type of investigation would require simulating boxes with more than 100 nm of length in the z-axis, which is too demanding for

https://doi.org/10.1021/acschemneuro.4c00333
ACS Chem. Neurosci. 2024, 15, 3354−3362

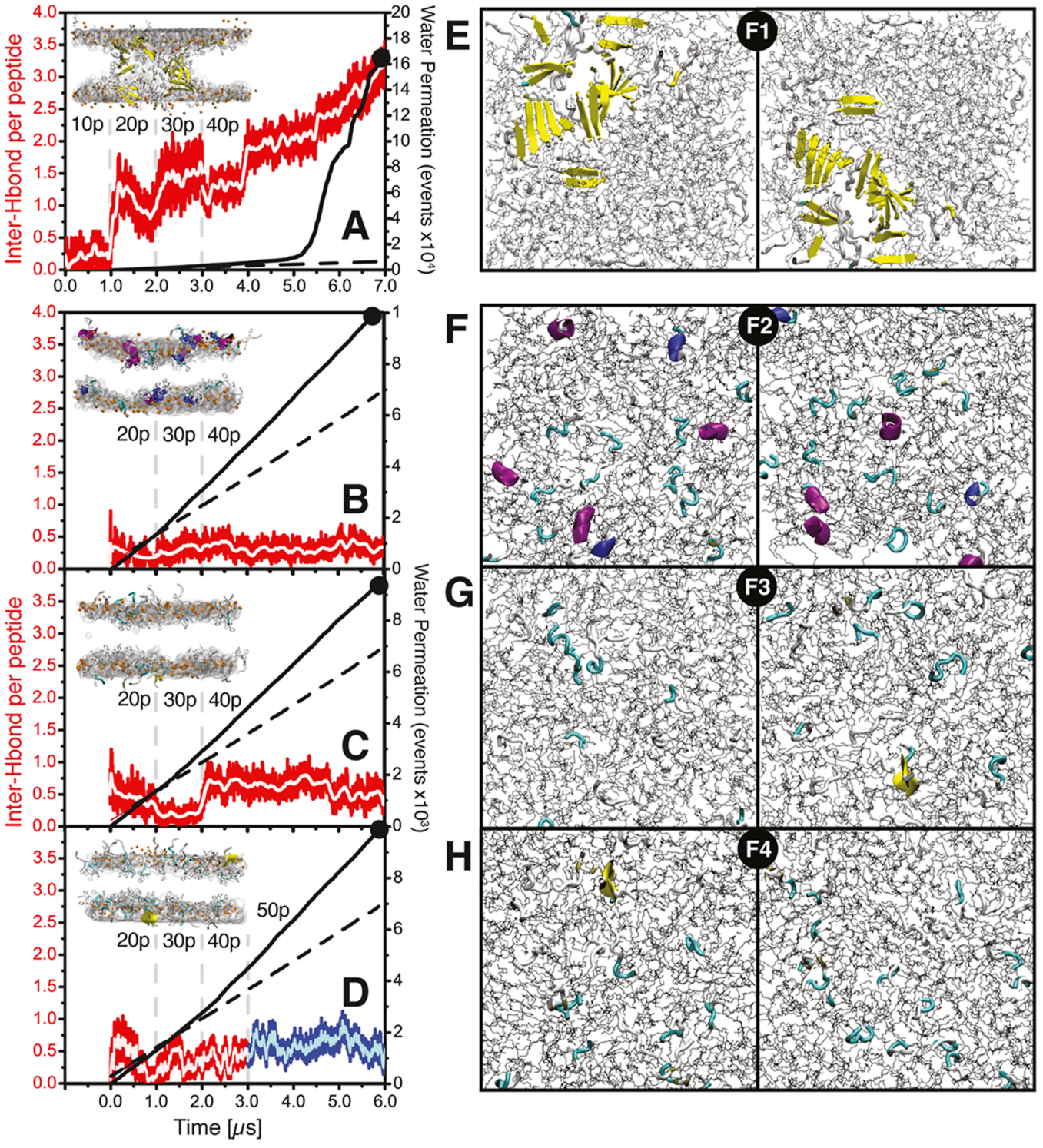

Figure 2. Peptide aggregation and water permeation across a lipid bilayer. The number of interbackbone hydrogen bonds (red) and water permeation (black) for simulations performed with (A) F1, (B) F2, (C) F3, and (D) F4 peptides. Dashed black lines correspond to the permeation in the absence of peptides. Vertical gray lines show the instant when 10 peptides are added to the simulation. (Inset) Cross-section of the lipid membrane depicting phosphate atoms of lipid head-groups (in orange), peptides (in cartoon representation), and water molecules (in gray) within the bilayer. The inset is reproduced in a larger format in Figure S4. (E−H) Last conformation of peptides on the upper and lower leaflets. Yellow, purple, blue, cyan, and white are used to represent β-sheets, α-helix, 3−10 helix, turn, and coil structures, respectively.

most available computers. To overcome this limitation, we perform simulations using a stepwise approach where N peptides are added gradually to the simulation box in order to mimic a situation in which the N peptides that are closer to the membrane are simulated first, followed by the next N peptides that are further away from the membrane.

Simulations are performed by consecutively adding N = 10 peptides to the solution and running a 1 μs simulation. This iterative process is carried out separately for peptides F1, F2,

https://doi.org/10.1021/acschemneuro.4c00333
ACS Chem. Neurosci. 2024, 15, 3354−3362

F3, and F4 (Figure 1) until the simulation box contains a total of 40 peptides, i.e., a 1:5 peptide/lipid ratio. Although adding more than 10 peptides to the solution in this iterative process could speed up membrane damage, we find that this results in the formation of F1 aggregates in solution, which do not disrupt the integrity of the lipid bilayer (Figure S1).

To quantify aggregation in our simulations, Figure 2A−D depicts the number N_{inter} (red lines) of interpeptide hydrogen bonds. This quantity increases systematically in simulations performed with F1 but not F2, F3, or F4 peptides, showing that only membrane-adsorbed F1 peptides aggregate. In an attempt to induce membrane damage, simulations for the F4 peptide were also performed at a higher concentration, i.e., by adding another 10 peptides to the solution, accounting for a peptide−lipid ratio of 1:4—blue line in panel D. To visualize these differences in aggregation, the second and third columns of Figure 2 depict the last configuration of upper and lower leaflets of the bilayer. Peptides F2, F3, and F4 are dispersed on both membrane leaflets, whereas F1 peptides are highly localized in space. In these panels, residues are colored based on their secondary structure: peptides F1, F2, and F3/F4 adopt mostly β-strands (yellow), helices (blue and purple), and coils/turns (white/cyan), respectively. This secondary structure content is quantified in Figure S2, and the segregation of nonpolar−polar residues is depicted in Figure S3 for the different peptides. The latter affects not only the secondary structure content but also the orientation of peptides with respect to the membrane surface, as shown in Figure S4.

Figure 2A−D also shows the number of N_{perm} (black full lines) of water permeation events in simulations performed with peptides F1 to F4. As a reference, black dashed lines depict permeation events in a bilayer without peptides. As peptides become adsorbed onto the membrane, they perturb its integrity, accounting for a rate of water permeation that is higher than for the pure membrane. This difference is visible in panels B−D for membranes with more than 30 adsorbed peptides. For F1 peptides (panel A), an abrupt change in the permeation rate accounting for 1 order of magnitude increase in N_{perm} is observed at around 5 μs as a pore forms on the membrane. The pore is depicted in the inset of panel A, where the cross-section of the bilayer shows β-sheets translocating across both leaflets. In contrast, the membrane remains intact for peptides F2, F3, and F4—insets of panels B−D. Insets are reproduced in Figure S6 in a larger format.

The picture that emerges from Figure 2 is that at low concentration, all peptides become adsorbed onto the membrane mostly as monomers. During the simulations, peptides F2, F3, and F4 remain dispersed mostly as monomers without aggregating significantly. This contrasts with the formation of β-sheets by F1 peptides, which penetrate the membrane, forming pore-like structures. The gradual aggregation of F1 peptides along the simulation is illustrated in Figure S5, showing the presence of only monomers at 1 μs, dimers at 2 μs, trimers at 3 μs, and larger aggregates at 4 μs.

To provide insights into the interactions accounting for aggregation, we identify the closest amino acids between pairs of peptides on the same leaflet as a function of their center-of-mass distance ξ. This analysis is performed for the last 0.5 μs of simulations performed with 10 peptides before aggregation takes place. Figure 3 shows the percentage of frames in the trajectory for which the closest atomic distances are between complementary charged amino acids (panel A) and nonpolar residues (panel B) as a function of ξ. As F1 peptides (black lines) approach each other, a distinguished peak emerges at ξ = 1.5 nm (panel A), showing that electrostatic interactions between E−K amino acids drive peptides to that distance in approximately 60% of the frames. This takes place at the expense of F−F interactions as the number of frames for which nonpolar residues are closer to each other becomes a minimum at that distance—panel B. As F1 peptides approach each other further (ξ < 1.5 nm), nonpolar residues become increasingly closer to each other, peaking at ξ = 1.0 nm. Characteristic configurations at ξ = 1.45 and 0.8 nm are depicted in panel C, showing oppositely charged and nonpolar residues interacting at these distances, respectively. Thus, Figure 3 provides evidence that F1 peptides are first attracted to each other via electrostatic interactions until they become close enough to allow nonpolar side chains to interact in the dry core of the bilayer. This interplay between electrostatic and nonpolar interactions does not take place for other peptides. In particular, electrostatic interactions between complementary charged residues become continuously more important as pairs of F2, F3, or F4 peptides approach each other without necessarily enabling nonpolar side chains to interact (Figure 3A,B). Characteristic structures for a pair of F4 peptides at different ξ distances are depicted in panel D, showing that conformations that optimize electrostatic interactions do not necessarily optimize nonpolar interactions. In particular, at ξ = 0.68 nm, charged residues are closer to each other than nonpolar ones, whereas the opposite is observed at ξ = 1.36 nm.

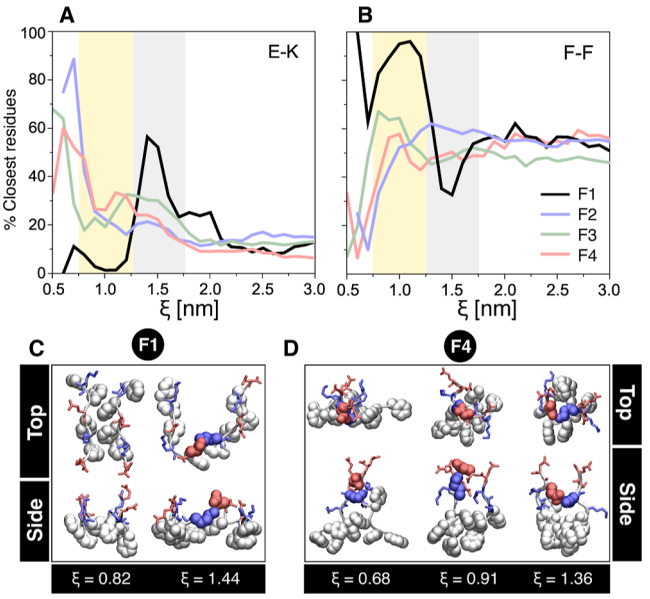

Figure 3. Interpeptide interactions at the water−lipid interface. Percentage of frames in which the closest residues between pairs of peptides are (A) oppositely charged or (B) nonpolar amino acids as a function of their center-of-mass distance ξ. Characteristic configurations of (C) F1 and (D) F4 peptides at different ξ distances viewed from the top and side of the membrane. Distances where F−F and E−K interactions dominate for F1 peptides are highlighted using yellow and gray shades, respectively.

Figure 4 shows how adsorbed F1 and F4 peptides affect the structure of the membrane by depicting the deuterium order parameter—S_{CH} computed for the different methylene groups of 1-palmitoyl-2-oleoyl-*sn*-glycero-3-phosphocholine (POPC) and 1-palmitoyl-2-oleoyl-*sn*-glycero-3-phosphoglycerol (POPG). This quantity is defined as $S_{CH} = \langle 3\cos^2 \Theta - 1 \rangle /$

https://doi.org/10.1021/acschemneuro.4c00333
ACS Chem. Neurosci. 2024, 15, 3354−3362

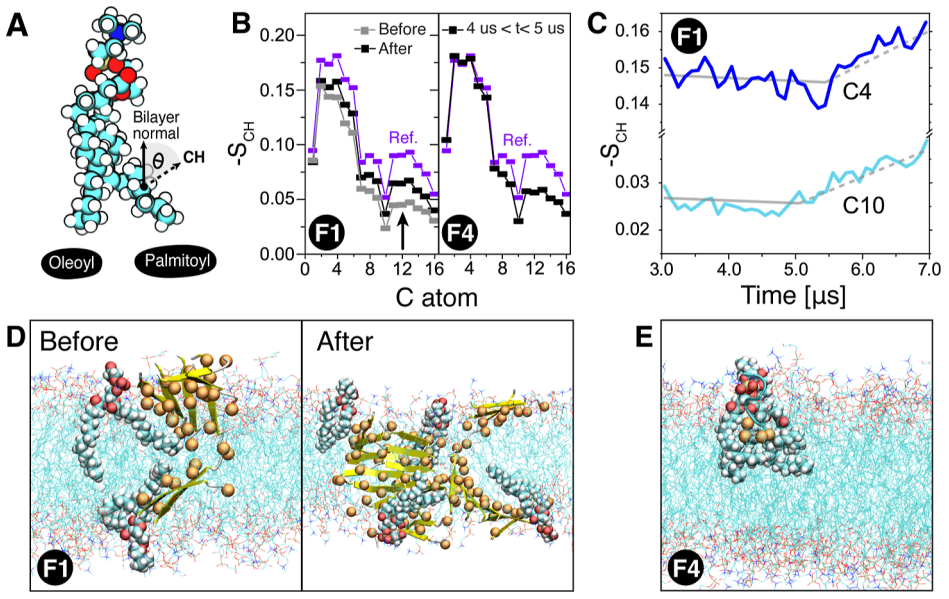

Figure 4. Effects of pore formation on the acyl-lipid tails. (A) Definition of the angle Θ used in the definition of the deuterium order parameter $S_{CH} = \langle 3\cos^2 \Theta - 1 \rangle / 2$. (B) Deuterium order parameter computed for a system without peptides (purple) and a membrane with adsorbed F1 (left) and F4 (right) peptides. The former was computed before (gray) and after (black) poration. (C) Time dependence of the deuterium order parameter computed in simulations with F1 peptides at the fourth and tenth methylene groups of POPC and POPG lipid tails. Characteristic lipids around (D) β-sheets made from F1 peptides before (left) and after (right) poration and (E) for F4 peptides. The nonpolar side chains of F1 and F4 peptides are represented using an orange bead.

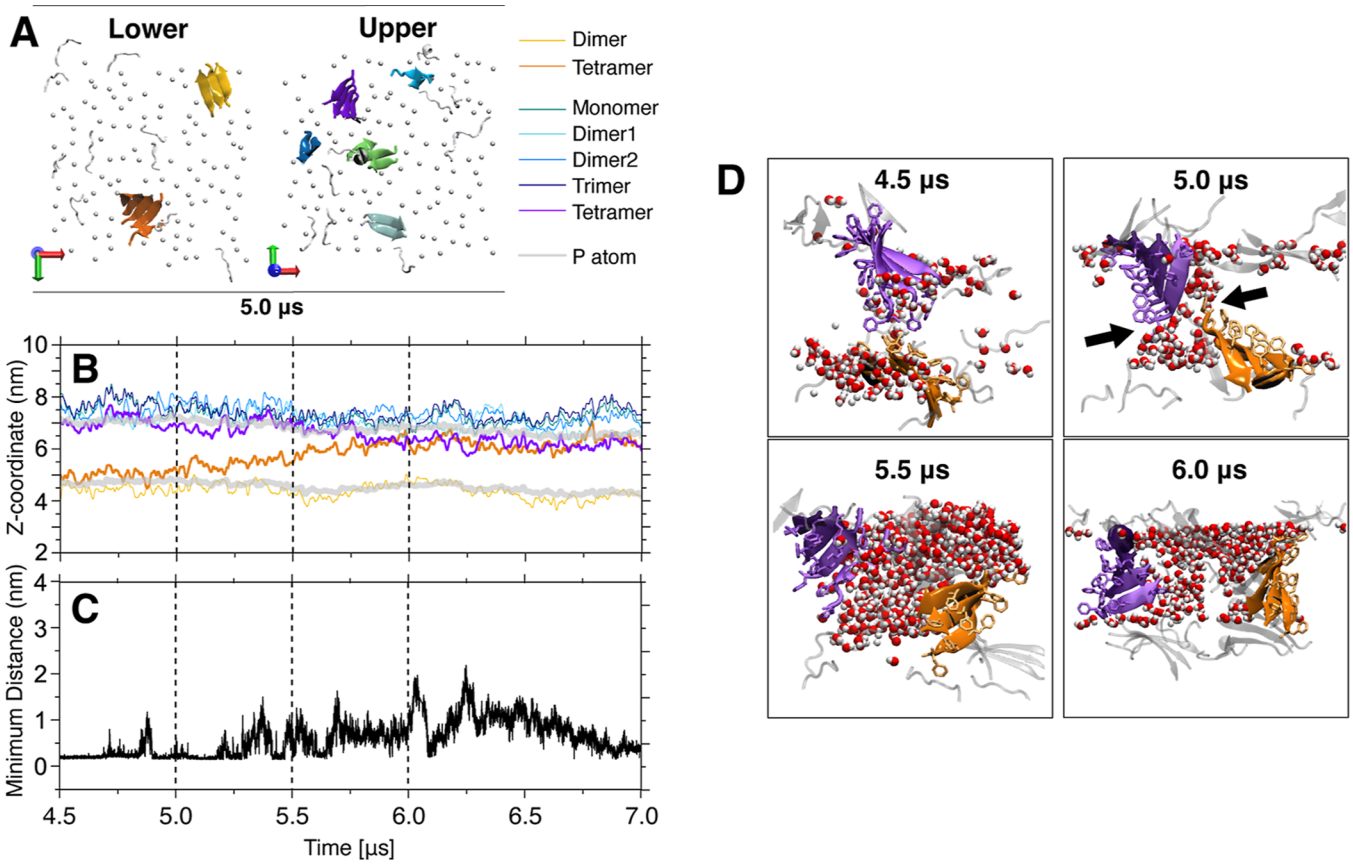

Figure 5. Pore formation. (A) Configuration of peptides on the lower and upper leaflets at 5.0 μs. (B) Time evolution of the z-coordinate of the center-of-mass of the different aggregates. (C) Minimal atomic distance between the two tetramers that penetrate the membrane surface. (D) Cross-section of the lipid membrane highlighting the two tetramers that penetrate the membrane at different instants of time. Water molecules within the bilayer are also shown.

https://doi.org/10.1021/acschemneuro.4c00333
ACS Chem. Neurosci. 2024, 15, 3354−3362

2, where Θ is the angle between carbon−hydrogen bonds of methylene groups and the bilayer normal[59] (Figure 4A). As a reference, S_{CH} computed for a 3:7 POPG/POPC membrane without adsorbed peptides is depicted in purple in Figure 4B. For both F1 and F4 peptides, adsorption onto the membrane surface accounts for a reduction in S_{CH} as lipid tails become more disordered to occupy empty spaces left by peptides within the bilayer (Figure 4D,E). Interestingly, pore formation reduces the degree of disorder in the membrane, i.e., S_{CH} increases—panel B. This takes place as the orientation of β-sheets changes from parallel to being perpendicular to the membrane surface as they penetrate the bilayer to delineate the pore walls (Figure 4D). In that configuration, nonpolar side chains of these β-sheets span the two leaflets of the bilayer, enabling neighboring acyl-lipid tails to be perpendicular to the membrane surface (Figure 4D). The time dependence of S_{CH} is depicted in panel C for two methylene groups in simulations performed with F1 peptides. It shows a continuous increase in S_{CH} starting at the instant peptides penetrate the bilayer, i.e., ∼5 μs. Thus, the formation of pores on the membrane allows it to become more ordered.

Figure 5A shows the color scheme used to depict the different aggregates on the upper and lower leaflets of the bilayer at time 5.0 μs. The *z*-coordinate of the center-of-mass of these aggregates is depicted in panel B, showing that poration starts with the two larger aggregates penetrating the bilayer, i.e., tetramers on the upper (purple) and lower (orange) leaflets. To characterize this process, panel C depicts the minimum atomic distance between these large aggregates. This distance is a minimum before and soon after the tetramers penetrate the membrane (4.5 μs < time < 5.25 μs), showing that they are hovering on top of each other. Visual inspection of the trajectory (4.5 μs in panel D) shows that, in this state, some of the edges of these β-sheets penetrate deep inside the membrane, allowing phenylalanine side chains on opposite leaflets to interact, stabilizing the tetramers on top of each other. Soon before penetrating the membrane (5 μs in panel D), water molecules bound to the polar faces of β-sheets are dragged to the middle of the bilayer from the lower and upper leaflets. This allows for the flow of water molecules across the membrane. Subsequently, the distance between tetramers increases, i.e., time 5.5 and 6.0 μs in panel D. In these configurations, β-sheets span both leaflets of the bilayer.

CONCLUSIONS

In summary, we find that the partitioning of polar and nonpolar side chains across the water−lipid interface determines the secondary structure and orientation of peptides with respect to the membrane surface. Peptides in which nonpolar and polar residues alternate along the sequence (F1) or are segregated to both extremities of the chain (F4) are preferentially oriented parallel or perpendicular to the membrane surface, respectively. Combining these nonpolar−polar patterns within the same sequence (F3) accounts for an intermediate orientation. Also, peptides that segregate nonpolar and polar residues to different faces of a helical wheel (F2) tend to fold into an α-helix. F1-labeled peptides self-assemble, and the larger aggregates (i.e., tetramers) form pores on the surface of lipid bilayers in the time frame of our simulation. Aggregation starts with long-range electrostatic interactions driving F1 peptides to intermediate distances from each other, where nonpolar side chains can interact. For F1 peptides at the water−lipid interface, these interactions are optimized when they adopt a β-sheet configuration that can be either parallel or antiparallel. This pattern of interaction wherein electrostatics is undertaken by short-range interactions is not observed for peptides F2, F3, and F4 and may explain the absence of aggregation on the bilayer surface.

Although β-sheets by F1 peptides are mostly parallel to the membrane, they can twist, and some of their edges penetrate deep inside the bilayer. This enables the nonpolar side chains of β-sheets on opposite leaflets to interact. Water molecules bound to charged side chains of these β-sheets are dragged to the middle of the bilayer, where they meet. This precedes poration in our simulations that started with the flow of a double file of water between polar faces of β-sheets. Consistent with these results, a combination of solid-state ^{15}N and ^{19}F NMR techniques was used to show that peptides, which lie flat on the surface of membranes, do not form pores, although they may disrupt the lipid bilayer via other mechanisms, e.g., via a carpeting effect.[60,61] This is the case for the cationic KL peptides made by alternating nonpolar leucine and positively charged lysine residues along the sequence. Thus, some degree of β-sheet twist may be required to allow for peptides to penetrate the bilayer. In our simulations, additional peptides became incorporated onto these partially penetrated β-sheets, which ended up spanning both leaflets of the bilayer without forming a complete β-barrel. Accordingly, the distance between β-sheets and the number of water molecules between them changed during the simulation.

For all of the systems studied here, adsorption increases the amount of disorder in the lipid membrane as acyl-lipid tails tend to occupy voids left by peptides within the bilayer. For F1 peptides, acyl-lipid tails wrap themselves around nonpolar faces of β-sheets to occupy the space left underneath these sheets that are initially oriented parallel to the membrane. Pore formation minimizes this type of disorder as β-sheets penetrate the membrane to become mostly perpendicular to the membrane surface.

In conclusion, our simulations show that an orchestrated interplay between nonpolar and polar interactions is required to account for β-sheet formation at the water−lipid interface and to allow these sheets to penetrate the membrane. Thus, pore formation is strongly affected by the nonpolar−polar sequence pattern that determines this interplay. We anticipate that a better understanding of how this pattern encodes for the structure of aggregates on the membrane surface will provide the needed insights to predict and control amyloid-induced membrane toxicity. This requires studying sequences that more closely mimic the nonpolar−polar sequence pattern of amyloid peptides. This may include sequences with five nonpolar residues flanked by charged residues, as in the case of $A\beta_{16-22}$. Moreover, we found that the partial penetration of water molecules escorted to the middle of the bilayer by polar faces of β-sheets starts poration by enabling the flow of one or two layers of water. We also observed that the level of membrane disorder induced by adsorbed peptides is reduced when pores are formed in our simulations, which may explain the stability of pore-like structures.

Although the unbiased simulations performed in this study, lasting ∼6 to 7 μs, are relatively long compared to similar simulations in the literature, they represent only a small fraction of the time elapsed in comparable experiments (typically 0.5−2 h). This raises the question of what would happen if the simulations were extended further. One may speculate that extending simulations with F1 peptides would

https://doi.org/10.1021/acschemneuro.4c00333
ACS Chem. Neurosci. 2024, 15, 3354−3362

allow pores to reorganize themselves into continuous β-barrels without dangling hydrogen bonds at the edges of existing β-sheets. As a result, pores would become more stable, reducing their likelihood of becoming annihilated. For peptides F2 to F4, Figure S1A indicates that small aggregates formed in solution tend to dissolve into smaller clusters when in contact with the membrane. This suggests that extending these simulations would not result in the formation of pores or aggregates at the water−lipid interface. Therefore, the results in this study are expected to be robust despite the shorter time scale of simulations compared to experiments.

METHODS

System Preparation. In this study, we use a model membrane made of 140 zwitterionic POPC and 60 negatively charged POPG lipids, i.e., a 7:3 POPC/POPG ratio. Although mammalian cells are less negative than the model membrane used in this study, a previous investigation reported a significant increase in adsorption when negative POPG lipids are added to zwitterionic membranes.[48] Therefore, our choice of model membrane promotes the scenario that we want to investigate where peptides adsorb on the membrane as monomers or small molecular weight aggregates instead of aggregating into fibril-like structures in solution, which are less toxic. It will be interesting in the future to study model membranes containing negative lipids that are more frequently found in mammalian cells and cholesterol. The membrane was prepared using the CHARMM-GUI suite, solvated using TIP3P water, and the charge of the system was neutralized by adding 60 sodium ions to the solution.[62−67]

The four peptides studied here are made using the same amino acids, which are 4 Phe (F), 2 Lys (K), and 2 Glu (E) residues. The sequence of these neutral amphipathic peptides is Ac-FKFEFKFE-NH_2 (F1), Ac-FFKKFFEE-NH_2 (F2), Ac-FFFKFEKE-NH_2 (F3), and Ac-FFFFKKEE-NH_2 (F4) (Figure 1). The label used for these peptides (i.e., F1 to F4) refers to the number of consecutive F residues at the N-terminal of the sequence.

The CHARMM36m force field is used to account for the atomic interactions in our simulation.[68] The initial box size was 9.0 × 9.0 × 12.5 nm^3, which accommodates ∼20, 000 TIP3P water molecules.[69]

Simulation Protocol. All-atom simulations were performed using GROMACS-2020.[70] The equations of motion were integrated using the leapfrog algorithm with a 2 fs time step. Electrostatic interactions were treated using the particle mesh Ewald technique with a Fourier grid spacing of 0.12 nm and a short-range cutoff of 1.0 nm.[71] A Lennard-Jones cutoff distance of 1.2 nm was used. Simulations were performed in the *NPT* ensemble. The Nośe−Hoover thermostat (τ_T = 1 ps) was used to maintain the temperature of the membrane, solvent, and peptides at 350 K.[72,73] This high temperature facilitates the adsorbing of peptides onto the membrane without accounting for their aggregation—see Figure S0. The semi-isotropic Parrinello−Rahman barostat (τ_P = 5 ps) was used to maintain the pressure in the system at 1 atm.[74,75]

Simulations were initially performed to equilibrate the solvated membrane without any peptides. Ten or 20 peptides were subsequently embedded in the solution, and a 1 μs simulation was conducted. This was followed by embedding 10 additional peptides into the solution and running a 1 μs simulation 2 and 3 times for peptides F2 and F3 and F1 and F4, respectively. The simulations were subsequently extended for 4 μs for peptide F1 and 3 μs for peptides F2, F3, and F4.

Analysis. All trajectories were analyzed by using GROMACS tools and custom in-house scripts. Hydrogen bonds were defined using the conventional 30° cutoff angle for H−D−A interactions and the 0.35 nm cutoff for the D−A distances. Deuterium order parameters were computed using the GROMACS gmx order command. Water permeation events were computed using an in-house code, which tracks water molecules as they transition from one leaflet to the middle of the bilayer to the other leaflet.[76−78]

ASSOCIATED CONTENT

Supporting Information

The Supporting Information is available free of charge at https://pubs.acs.org/doi/10.1021/acschemneuro.4c00333.

Comparison of how the different peptides adsorb as opposed to aggregate in solution, structural analysis of adsorbed peptides, and visual inspection of adsorbed F1 peptides along the simulation (PDF)

AUTHOR INFORMATION

Corresponding Author

Cristiano L. Dias − *Department of Physics, New Jersey Institute of Technology, Newark, New Jersey 07102-1982, United States;* orcid.org/0000-0002-8765-3922; Email: cld@njit.edu

Authors

Warin Rangubpit − *Department of Physics, New Jersey Institute of Technology, Newark, New Jersey 07102-1982, United States*

Siwaporn Sungted − *Department of Physics, Faculty of Science, Kasetsart University, Bangkok 10900, Thailand; Computational Biomodelling Laboratory for Agricultural Science and Technology (CBLAST), Faculty of Science, Kasetsart University, Bangkok 10900, Thailand*

Jirasak Wong-Ekkabut − *Department of Physics, Faculty of Science, Kasetsart University, Bangkok 10900, Thailand; Computational Biomodelling Laboratory for Agricultural Science and Technology (CBLAST), Faculty of Science, Kasetsart University, Bangkok 10900, Thailand*

Hannah E. Distaffen − *Department of Chemistry, University of Rochester, Rochester, New York 14627-0216, United States*

Bradley L. Nilsson − *Department of Chemistry, University of Rochester, Rochester, New York 14627-0216, United States; Materials Science Program, University of Rochester, Rochester, New York 14627-0166, United States;* orcid.org/0000-0003-1193-3693

Complete contact information is available at: https://pubs.acs.org/10.1021/acschemneuro.4c00333

Author Contributions

W.R. and C.L.D. designed the experiments; W.R. and S.S. executed the experiments; W.R. performed the analysis; W.R. and C.L.D. wrote the paper; J.W., H.D., and B.N. reviewed and edited the paper.

Notes

The authors declare no competing financial interest.

ACKNOWLEDGMENTS

C.L.D., W.R., H.D., and B.N. are supported by the National Institute of General Medical Health under grant no. 1R15GM148982-01. Computational resources were provided by the Academic and Research Computing System (ARCS) at the New Jersey Institute of Technology. J.W. is supported by the National Research Council of Thailand (NRCT) through the Research Grants for Talented Mid-Career Researchers with grant no. N41A640080 and the National Science Research and Innovation Fund (NSRF) via the Program Management Unit for Human Resources and Institutional Development, Research and Innovation [grant no. B42G670041].

REFERENCES

(1) Kampmann, M. Molecular and cellular mechanisms of selective vulnerability in neurodegenerative diseases. *Nat. Rev. Neurosci.* **2024**, *25*, 351−371.

(2) Dobson, C. M.; Knowles, T. P. J.; Vendruscolo, M. The Amyloid Phenomenon and Its Significance in Biology and Medicine. *Cold Spring Harbor Perspect. Biol.* **2020**, *12*, a033878.

(3) Hampel, H.; Hardy, J.; Blennow, K.; Chen, C.; Perry, G.; Kim, S. H.; Villemagne, V. L.; Aisen, P.; Vendruscolo, M.; Iwatsubo, T.; Masters, C. L.; Cho, M.; Lannfelt, L.; Cummings, J. L.; Vergallo, A. The Amyloid-β Pathway in Alzheimer's Disease. *Mol. Psychiatr.* **2021**, *26*, 5481−5503.

(4) Andrade, S.; Loureiro, J. A.; Pereira, M. C. The Role of Amyloid β-Biomembrane Interactions in the Pathogenesis of Alzheimer's Disease: Insights from Liposomes as Membrane Models. *ChemPhysChem* **2021**, *22*, 1547−1565.

(5) Viles, J. H. Imaging Amyloid-β Membrane Interactions: Ion-Channel Pores and Lipid-Bilayer Permeability in Alzheimer's Disease. *Angew. Chem., Int. Ed.* **2023**, *62*, No. e202215785.

(6) Soscia, S. J.; Kirby, J. E.; Washicosky, K. J.; Tucker, S. M.; Ingelsson, M.; Hyman, B.; Burton, M. A.; Goldstein, L. E.; Duong, S.; Tanzi, R. E.; Moir, R. D. The Alzheimer's Disease-Associated Amyloid β-Protein Is an Antimicrobial Peptide. *PLoS One* **2010**, *5*, No. e9505.

(7) Buchanan, J. A.; Varghese, N. R.; Johnston, C. L.; Sunde, M. Functional Amyloids: Where Supramolecular Amyloid Assembly Controls Biological Activity or Generates New Functionality. *J. Mol. Biol.* **2023**, *435*, 167919.

(8) Myers, C.; Cornwall, G. A. Host defense amyloids: Biosensors of the immune system? *Andrology* **2024**, *12*, 973.

(9) Lashuel, H. A.; Lansbury, P. T. Are amyloid diseases caused by protein aggregates that mimic bacterial pore-forming toxins? *Q. Rev. Biophys.* **2006**, *39*, 167−201.

(10) Lee, E. Y.; Srinivasan, Y.; de Anda, J.; Nicastro, L. K.; Tükel, Ç.; Wong, G. C. L. Functional Reciprocity of Amyloids and Antimicrobial Peptides: Rethinking the Role of Supramolecular Assembly in Host Defense, Immune Activation, and Inflammation. *Front. Immunol.* **2020**, *11*, 1629.

(11) Ilie, I. M.; Caflisch, A. Simulation Studies of Amyloidogenic Polypeptides and Their Aggregates. *Chem. Rev.* **2019**, *119*, 6956−6993.

(12) Morriss-Andrews, A.; Brown, F. L. H.; Shea, J.-E. A Coarse-Grained Model for Peptide Aggregation on a Membrane Surface. *J. Phys. Chem. B* **2014**, *118*, 8420−8432.

(13) Morriss-Andrews, A.; Shea, J.-E. Simulations of Protein Aggregation: Insights from Atomistic and Coarse-Grained Models. *J. Phys. Chem. Lett.* **2014**, *5*, 1899−1908.

(14) Wang, Y.; Bunce, S. J.; Radford, S. E.; Wilson, A. J.; Auer, S.; Hall, C. K. Thermodynamic phase diagram of amyloid-β (16−22) peptide. *Proc. Natl. Acad. Sci. U.S.A.* **2019**, *116*, 2091−2096.

(15) Pellarin, R.; Caflisch, A. Interpreting the Aggregation Kinetics of Amyloid Peptides. *J. Mol. Biol.* **2006**, *360*, 882−892.

(16) Sahoo, A.; Matysiak, S. Effects of applied surface-tension on membrane-assisted Aβ aggregation. *Phys. Chem. Chem. Phys.* **2021**, *23*, 20627−20633.

(17) Barz, B.; Urbanc, B. Minimal Model of Self-Assembly: Emergence of Diversity and Complexity. *J. Phys. Chem. B* **2014**, *118*, 3761−3770.

(18) Saric, A.; Michaels, T. C. T.; Zaccone, A.; Knowles, T. P. J.; Frenkel, D. Kinetics of spontaneous filament nucleation via oligomers: Insights from theory and simulation. *J. Chem. Phys.* **2016**, *145*, 211926.

(19) Krausser, J.; Knowles, T. P. J.; Šarić, A. Physical mechanisms of amyloid nucleation on fluid membranes. *Proc. Natl. Acad. Sci. U.S.A.* **2020**, *117*, 33090−33098.

(20) Michaels, T. C. T.; Saric, A.; Curk, S.; Bernfur, K.; Arosio, P.; Meisl, G.; Dear, A. J.; Cohen, S. I. A.; Dobson, C. M.; Vendruscolo, M.; Linse, S.; Knowles, T. P. J. Dynamics of oligomer populations formed during the aggregation of Alzheimer's Aβ42 peptide. *Nat. Chem.* **2020**, *12*, 445−451.

(21) Kabelka, I.; Vácha, R. Advances in Molecular Understanding of α-Helical Membrane-Active Peptides. *Acc. Chem. Res.* **2021**, *54*, 2196−2204.

(22) Wang, Y.; Chen, C. H.; Hu, D.; Ulmschneider, M. B.; Ulmschneider, J. P. Spontaneous formation of structurally diverse membrane channel architectures from a single antimicrobial peptide. *Nat. Commun.* **2016**, *7*, 13535.

(23) Upadhyay, S. K.; Wang, Y.; Zhao, T.; Ulmschneider, J. P. Insights from Micro-second Atomistic Simulations of Melittin in Thin Lipid Bilayers. *J. Membr. Biol.* **2015**, *248*, 497−503.

(24) Perrin, B. S.; Fu, R.; Cotten, M. L.; Pastor, R. W. Simulations of Membrane-Disrupting Peptides II: AMP Piscidin 1 Favors Surface Defects over Pores. *Biophys. J.* **2016**, *111*, 1258−1266.

(25) Chen, C. H.; Melo, M. C.; Berglund, N.; Khan, A.; de la Fuente-Nunez, C.; Ulmschneider, J. P.; Ulmschneider, M. B. Understanding and modelling the interactions of peptides with membranes: from partitioning to self-assembly. *Curr. Opin. Struct. Biol.* **2020**, *61*, 160−166.

(26) Lipkin, R.; Pino-Angeles, A.; Lazaridis, T. Transmembrane Pore Structures of β-Hairpin Antimicrobial Peptides by All-Atom Simulations. *J. Phys. Chem. B* **2017**, *121*, 9126−9140.

(27) Sepehri, A.; Nepal, B.; Lazaridis, T. Distinct Modes of Action of IAPP Oligomers on Membranes. *J. Chem. Inf. Model.* **2021**, *61*, 4645−4655.

(28) Dutta, A.; Sepehri, A.; Lazaridis, T. Putative Pore Structures of Amyloid β 25−35 in Lipid Bilayers. *Biochemistry* **2023**, *62*, 2549−2558.

(29) Sepehri, A.; Lazaridis, T. Putative Structures of Membrane-Embedded Amyloid β Oligomers. *ACS Chem. Neurosci.* **2023**, *14*, 99−110.

(30) Maurer, M.; Lazaridis, T. Transmembrane β-Barrel Models of α-Synuclein Oligomers. *J. Chem. Inf. Model.* **2023**, *63*, 7171−7179.

(31) Yang, Y.; Distaffen, H.; Jalali, S.; Nieuwkoop, A. J.; Nilsson, B. L.; Dias, C. L. Atomic Insights into Amyloid-Induced Membrane Damage. *ACS Chem. Neurosci.* **2022**, *13*, 2766−2777.

(32) Fatafta, H.; Khaled, M.; Owen, M. C.; Sayyed-Ahmad, A.; Strodel, B. Amyloid-β peptide dimers undergo a random coil to β-sheet transition in the aqueous phase but not at the neuronal membrane. *Proc. Natl. Acad. Sci. U.S.A.* **2021**, *118*, No. e2106210118.

(33) Banerjee, S.; Hashemi, M.; Zagorski, K.; Lyubchenko, Y. L. Cholesterol in Membranes Facilitates Aggregation of Amyloid β Protein at Physiologically Relevant Concentrations. *ACS Chem. Neurosci.* **2021**, *12*, 506−516.

(34) Ermilova, I.; Lyubartsev, P. Modelling of interactions between Aβ(25−35) peptide and phospholipid bilayers: effects of cholesterol and lipid saturation. *RSC Adv.* **2020**, *10*, 3902−3915.

(35) Zhang, X.; Clair, J. R.; London, E.; Raleigh, D. P. Islet Amyloid Polypeptide Membrane Interactions: Effects of Membrane Composition. *Biochemistry* **2017**, *56*, 376−390.

(36) Yang, M.; Wang, K.; Lin, J.; Wang, L.; Wei, F.; Zhu, J.; Zheng, W.; Shen, L. Gel Phase Membrane Retards Amyloid β-Peptide (1−42) Fibrillation by Restricting Slaved Diffusion of Peptides on Lipid Bilayers. *Langmuir* **2018**, *34*, 8408−8414.

(37) Galvagnion, C.; Brown, J. W. P.; Ouberai, M. M.; Flagmeier, P.; Vendruscolo, M.; Buell, A. K.; Sparr, E.; Dobson, C. M. Chemical properties of lipids strongly affect the kinetics of the membrane-induced aggregation of α-synuclein. *Proc. Natl. Acad. Sci. U.S.A.* **2016**, *113*, 7065−7070.

(38) O'Leary, E. I.; Jiang, Z.; Strub, M.-P.; Lee, J. C. Effects of phosphatidylcholine membrane fluidity on the conformation and aggregation of N-terminally acetylated α-synuclein. *J. Biol. Chem.* **2018**, *293*, 11195−11205.

(39) Nuscher, B.; Kamp, F.; Mehnert, T.; Odoy, S.; Haass, C.; Kahle, P. J.; Beyer, K. α-Synuclein Has a High Affinity for Packing Defects in a Bilayer Membrane: A THERMODYNAMICS STUDY. *J. Biol. Chem.* **2004**, *279*, 21966−21975.

(40) Nilsson, B. L.; Celebi Torabfam, G.; Dias, C. L. Peptide Self-Assembly into Amyloid Fibrils: Unbiased All-Atom Simulations. *J. Phys. Chem. B* **2024**, *128*, 3320−3328.

https://doi.org/10.1021/acschemneuro.4c00333
ACS Chem. Neurosci. 2024, 15, 3354−3362

(41) Marini, D. M.; Hwang, W.; Lauffenburger, D. A.; Zhang, S.; Kamm, R. D. Left-Handed Helical Ribbon Intermediates in the Self-Assembly of a β-Sheet Peptide. *Nano Lett.* **2002**, *2*, 295−299.
(42) Swanekamp, R. J.; DiMaio, J. T. M.; Bowerman, C. J.; Nilsson, B. L. Coassembly of Enantiomeric Amphipathic Peptides into Amyloid-Inspired Rippled β-Sheet Fibrils. *J. Am. Chem. Soc.* **2012**, *134*, 5556−5559.
(43) Wang, F.; Gnewou, O.; Wang, S.; Osinski, T.; Zuo, X.; Egelman, E. H.; Conticello, V. P. Deterministic chaos in the self-assembly of β sheet nanotubes from an amphipathic oligopeptide. *Matter* **2021**, *4*, 3217−3231.
(44) Jalali, S.; Yang, Y.; Mahmoudinobar, F.; Singh, S. M.; Nilsson, B. L.; Dias, C. Using all-atom simulations in explicit solvent to study aggregation of amphipathic peptides into amyloid-like fibrils. *J. Mol. Liq.* **2022**, *347*, 118283.
(45) Jalali, S.; Zhang, R.; Haataja, M. P.; Dias, C. L. Nucleation and Growth of Amyloid Fibrils. *J. Phys. Chem. B* **2023**, *127*, 9759−9770.
(46) Zhang, R.; Jalali, S.; Dias, C.; Haataja, M. P. Growth kinetics of amyloid-like fibrils: An integrated atomistic simulation and continuum theory approach. *PNAS Nexus* **2024**, *3*, 045.
(47) Yang, Y.; Dias, C. L. Peptide−Membrane Binding: Effects of the Amino Acid Sequence. *J. Phys. Chem. B* **2023**, *127*, 912−920.
(48) Yang, Y.; Jalali, S.; Nilsson, B. L.; Dias, C. L. Binding Mechanisms of Amyloid-like Peptides to Lipid Bilayers and Effects of Divalent Cations. *ACS Chem. Neurosci.* **2021**, *12*, 2027−2035.
(49) Dias, C. L.; Jalali, S.; Yang, Y.; Cruz, L. Role of Cholesterol on Binding of Amyloid Fibrils to Lipid Bilayers. *J. Phys. Chem. B* **2020**, *124*, 3036−3042.
(50) Javanainen, M.; Melcrová, A.; Magarkar, A.; Jurkiewicz, P.; Hof, M.; Jungwirth, P.; Martinez-Seara, H. Two cations, two mechanisms: interactions of sodium and calcium with zwitterionic lipid membranes. *Chem. Commun.* **2017**, *53*, 5380−5383.
(51) Sciacca, M. F. M.; Monaco, I.; La Rosa, C.; Milardi, D. The active role of Ca^{2+} ions in Aβ-mediated membrane damage. *Chem. Commun.* **2018**, *54*, 3629−3631.
(52) Sciacca, M. F. M.; Milardi, D.; Messina, G. M. L.; Marletta, G.; Brender, J. R.; Ramamoorthy, A.; La Rosa, C. Cations as Switches of Amyloid-Mediated Membrane Disruption Mechanisms: Calcium and IAPP. *Biophys. J.* **2013**, *104*, 173−184.
(53) Engel, M. F. M.; Khemtémourian, L.; Kleijer, C. C.; Meeldijk, H. J. D.; Jacobs, J.; Verkleij, A. J.; de Kruijff, B.; Killian, J. A.; Höppener, J. W. M. Membrane damage by human islet amyloid polypeptide through fibril growth at the membrane. *Proc. Natl. Acad. Sci. U.S.A.* **2008**, *105*, 6033−6038.
(54) Arispe, N.; Pollard, H. B.; Rojas, E. Giant multilevel cation channels formed by Alzheimer disease amyloid beta-protein [A beta P-(1−40)] in bilayer membranes. *Proc. Natl. Acad. Sci. U.S.A.* **1993**, *90*, 10573−10577.
(55) Quist, A.; Doudevski, I.; Lin, H.; Azimova, R.; Ng, D.; Frangione, B.; Kagan, B.; Ghiso, J.; Lal, R. Amyloid ion channels: A common structural link for protein-misfolding disease. *Proc. Natl. Acad. Sci. U.S.A.* **2005**, *102*, 10427−10432.
(56) Ulmschneider, J. P.; Ulmschneider, M. B. Molecular Dynamics Simulations Are Redefining Our View of Peptides Interacting with Biological Membranes. *Acc. Chem. Res.* **2018**, *51*, 1106−1116.
(57) Lipkin, R.; Lazaridis, T. Computational studies of peptide-induced membrane pore formation. *Philos. Trans. R. Soc. Lond. B Biol. Sci.* **2017**, *372*, 20160219.
(58) Voelker, M. J.; Barz, B.; Urbanc, B. Fully Atomistic Aβ40 and Aβ42 Oligomers in Water: Observation of Porelike Conformations. *J. Chem. Theory Comput.* **2017**, *13*, 4567−4583.
(59) Piggot, T. J.; Allison, J. R.; Sessions, R. B.; Essex, J. W. On the Calculation of Acyl Chain Order Parameters from Lipid Simulations. *J. Chem. Theory Comput.* **2017**, *13*, 5683−5696.
(60) Schweigardt, F.; Strandberg, E.; Wadhwani, P.; Reichert, J.; Bürck, J.; Cravo, H. L. P.; Burger, L.; Ulrich, A. S. Membranolytic Mechanism of Amphiphilic Antimicrobial β-Stranded [KL]n Peptides. *Biomedicines* **2022**, *10*, 2071.
(61) Strandberg, E.; Schweigardt, F.; Wadhwani, P.; Bürck, J.; Reichert, J.; Cravo, H. L. P.; Burger, L.; Ulrich, A. S. Phosphate-dependent aggregation of [KL]n peptides affects their membranolytic activity. *Sci. Rep.* **2020**, *10*, 12300.
(62) Wu, E. L.; Cheng, X.; Jo, S.; Rui, H.; Song, K. C.; Dávila-Contreras, E. M.; Qi, Y.; Lee, J.; Monje-Galvan, V.; Venable, R. M.; Klauda, J. B.; Im, W. CHARMM-GUI Membrane Builder toward realistic biological membrane simulations. *J. Comput. Chem.* **2014**, *35*, 1997−2004.
(63) Jo, S.; Lim, J. B.; Klauda, J. B.; Im, W. CHARMM-GUI Membrane Builder for Mixed Bilayers and Its Application to Yeast Membranes. *Biophys. J.* **2009**, *97*, 50−58.
(64) Lee, J.; Patel, D. S.; Ståhle, J.; Park, S.-J.; Kern, N. R.; Kim, S.; Lee, J.; Cheng, X.; Valvano, M. A.; Holst, O.; et al. CHARMM-GUI Membrane Builder for Complex Biological Membrane Simulations with Glycolipids and Lipoglycans. *J. Chem. Theory Comput.* **2019**, *15*, 775−786.
(65) Jo, S.; Kim, T.; Im, W. Automated Builder and Database of Protein/Membrane Complexes for Molecular Dynamics Simulations. *PLoS One* **2007**, *2*, e880−e889.
(66) Jo, S.; Kim, T.; Iyer, V. G.; Im, W. CHARMM-GUI: A web-based graphical user interface for CHARMM. *J. Comput. Chem.* **2008**, *29*, 1859−1865.
(67) Brooks, B. R.; Brooks, C. L., III; Mackerell, A. D., Jr.; Nilsson, L.; Petrella, R. J.; Roux, B.; Won, Y.; Archontis, G.; Bartels, C.; Boresch, S.; et al. CHARMM: The biomolecular simulation program. *J. Comput. Chem.* **2009**, *30*, 1545−1614.
(68) Lee, J.; Cheng, X.; Swails, J. M.; Yeom, M. S.; Eastman, P. K.; Lemkul, J. A.; Wei, S.; Buckner, J.; Jeong, J. C.; Qi, Y.; et al. CHARMM-GUI Input Generator for NAMD, GROMACS, AMBER, OpenMM, and CHARMM/OpenMM Simulations Using the CHARMM36 Additive Force Field. *J. Chem. Theory Comput.* **2016**, *12*, 405−413.
(69) Price, D. J.; Brooks, I.; Charles, L. A modified TIP3P water potential for simulation with Ewald summation. *J. Chem. Phys.* **2004**, *121*, 10096−10103.
(70) Lindahl, H.; Abraham; van der Spoel *GROMACS 2020 Manual*, 2020.
(71) Essmann, U.; Perera, L.; Berkowitz, M. L.; Darden, T.; Lee, H.; Pedersen, L. G. A smooth particle mesh Ewald method. *J. Chem. Phys.* **1995**, *103*, 8577−8593.
(72) Nosé, S. A molecular dynamics method for simulations in the canonical ensemble. *Mol. Phys.* **1984**, *52*, 255−268.
(73) Hoover, W. G. Canonical dynamics: Equilibrium phase-space distributions. *Phys. Rev. A: At., Mol., Opt. Phys.* **1985**, *31*, 1695−1697.
(74) Bussi, G.; Donadio, D.; Parrinello, M. Canonical sampling through velocity rescaling. *J. Chem. Phys.* **2007**, *126*, 014101.
(75) Parrinello, M.; Rahman, A. Polymorphic transitions in single crystals: A new molecular dynamics method. *J. Appl. Phys.* **1981**, *52*, 7182−7190.
(76) Hardiagon, A.; Murail, S.; Huang, L.-B.; van der Lee, A.; Sterpone, F.; Barboiu, M.; Baaden, M. Molecular dynamics simulations reveal statistics and microscopic mechanisms of water permeation in membrane-embedded artificial water channel nano-constructs. *J. Chem. Phys.* **2021**, *154*, 184102.
(77) Wong-ekkabut, J.; Karttunen, M. Molecular dynamics simulation of water permeation through the alpha-hemolysin channel. *J. Biol. Phys.* **2016**, *42*, 133−146.
(78) Boonnoy, P.; Karttunen, M.; Wong-ekkabut, J. Alpha-tocopherol inhibits pore formation in oxidized bilayers. *Phys. Chem. Chem. Phys.* **2017**, *19*, 5699−5704.

https://doi.org/10.1021/acschemneuro.4c00333
ACS Chem. Neurosci. 2024, 15, 3354−3362